Applied Thermal Engineering 31 (2011) 1332–1346

Contents lists available at ScienceDirect

Applied Thermal Engineering

journal homepage: www.elsevier.com/locate/apthermeng

Thermal radiators with embedded pulsating heat pipes: Infra-red thermography and simulations

Vadiraj A. Hemadri, Ashish Gupta, Sameer Khandekar*

Department of Mechanical Engineering, Indian Institute of Technology Kanpur, Kanpur, UP 208016, India

ARTICLE INFO

Article history:
Received 14 December 2010
Accepted 9 January 2011
Available online 18 January 2011

Keywords:
Pulsating heat pipes
Thermal radiators
Conjugate heat transfer
Infra-red thermography
Computational modeling

ABSTRACT

With the aim of exploring potential applications of Pulsating Heat Pipes (PHP), for space/terrestrial sectors, experimental study of embedded PHP thermal radiators, having two different effective Biot numbers respectively, and subjected to conjugate heat transfer conditions on their surface, i.e., natural convection and radiation, has been carried out under different thermo-mechanical boundary conditions. High resolution infrared camera is used to obtain spatial temperature profiles of the radiators. To complement the experimental study, detailed 3D computational heat transfer simulation has also been undertaken. By embedding PHP structures, it was possible to make the net thermal resistance of the mild steel radiator plate equivalent to the aluminum radiator plate, in spite of the large difference in their respective thermal conductivities ($k_{Al} \sim 4k_{MS}$). The study reveals that embedded PHP structures can be beneficial only under certain boundary conditions. The degree of isothermalization achieved in these structures strongly depends on its effective Biot number. The relative advantage of embedded PHP is appreciably higher if the thermal conductivity of the radiator plate material itself is low. The study indicates that the effective thermal conductivity of embedded PHP structure is of the order of 400 W/mK to 2300 W/mK, depending on the operating conditions.

1. Introduction

Thermal radiators are an essential part of any space sector application. At present, there are many proven space radiator systems, such as [1]:

- Passive structure/honeycomb panels
- Conventional heat pipe embedded structures
- Metal Matrix Composites (AlSiC, Graphite/Al)
- Variable area actively controlled radiators
- Liquid pumped loop (NH_3)
- Loop Heat Pipe (LHP)/Capillary Pumped Loops
- Smart radiators (Thermo-optical surface property variation)

Each design has some advantages and some shortcomings. The final choice of any one type depends on many factors such as, total heat load, flux levels, available area, payload capacity, structural requirements etc. Although the above designs meet the present requirements of the industry, future applications envisage higher heat flux levels. Although conventional wicked heat pipes have been routinely used for redistribution/transfer of heat on thermal radiator panels, the concept of using an embedded Pulsating Heat Pipe (PHP) for such an application is rather novel [2].[1] Embedded PHP structures for electronics cooling application have also been tested by Yang et al. [6], although their work did not have radiative or natural convective boundary conditions. In this work we investigate the thermal performance of two different radiator plates, having embedded PHP structures, using infrared thermography.

To understand the effectiveness of the embedded PHP system, let us first approach the problem with a 1-D simplified point of view, as depicted in Fig. 1(a). The heat transfer through the plate, along with the various resistances, is given by [7]:

$$\begin{aligned}(T_1 - T_2)/\dot{q}'' &= R_{th}|_{\text{conduction}} = L_C/k_{\text{plate}} \\ (T_2 - T_\infty)/\dot{q}'' &= R_{th}|_{\text{convection}} = h^{-1} \\ (T_2 - T_\infty)/\dot{q}'' &= R_{th}|_{\text{radiation}} = \left(4 \cdot \sigma_r \cdot T_m^3\right)^{-1}\end{aligned} \tag{1}$$

where,

* Corresponding author. Tel.: +91 512 2597038; fax: +91 512 2597408.
E-mail address: samkhan@iitk.ac.in (S. Khandekar).

[1] Interested readers may refer to [3–5] for understanding the operational characteristics and thermal behavior of pulsating heat pipes.

1359-4311/$ – see front matter © 2011 Elsevier Ltd. All rights reserved.
doi:10.1016/j.applthermaleng.2011.01.004

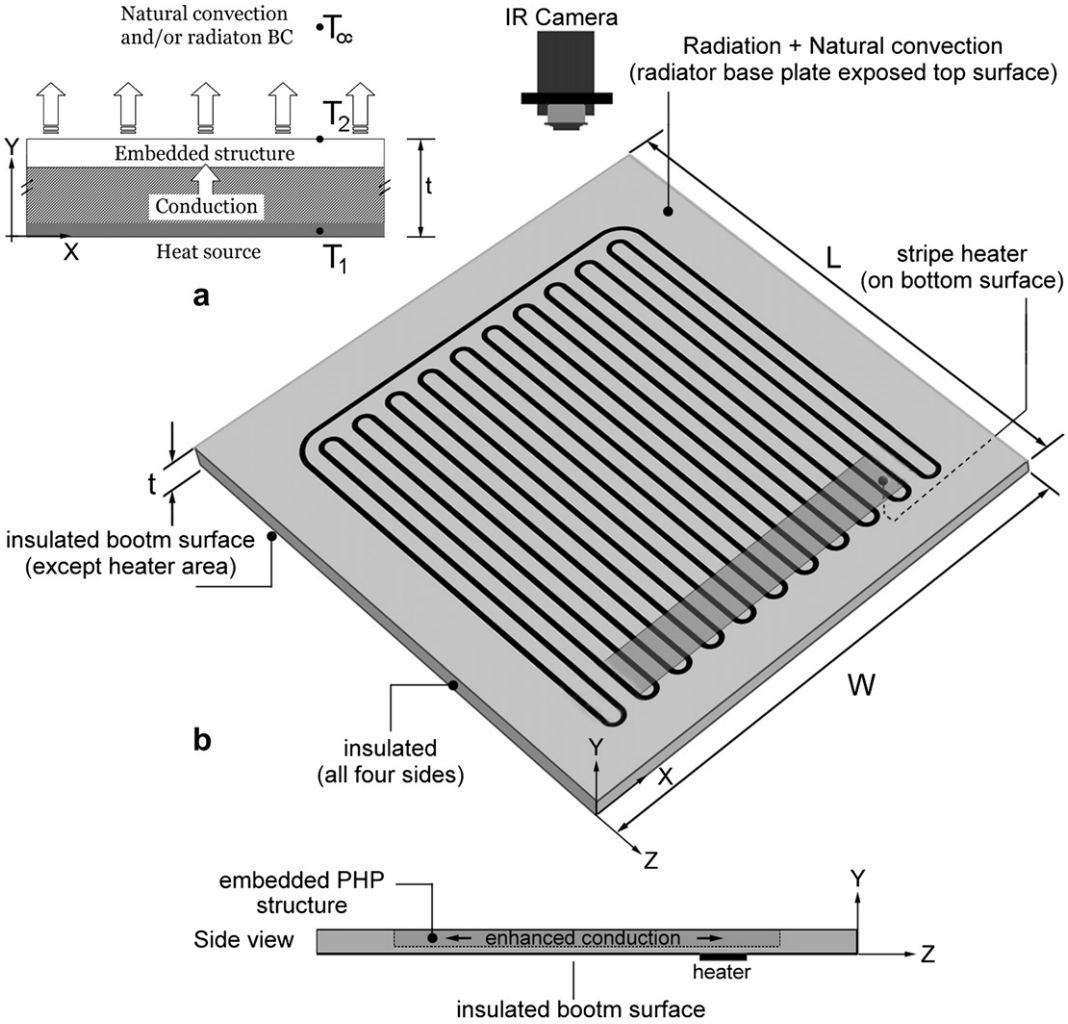

Fig. 1. (a) One-dimensional representation of the heat transfer through the radiator plate (b) Schematic representation of the radiator plate with embedded PHP, subjected to conjugate heat transfer, is shown here along with the experimental boundary conditions applicable on the plate.

$$T_m = \left[\frac{\left(T_2^2 + T_\infty^2\right)(T_2 + T_\infty)}{4}\right]^{1/3} \tag{2}$$

The effective Biot Number ($\overline{Bi}$) compares the internal thermal resistance of the plate to the total external heat transfer resistance, which in the present case is due to natural convection and radiation. (For space applications, only radiation boundary condition is applicable on the plate surface, while for terrestrial applications, both act simultaneously).

$$\overline{Bi} = \frac{\text{internal conductive resistance}}{\text{natural convective resistance} + \text{radiation}} = \frac{\left(L_C/k_{\text{plate}}\right)}{(1/h) + \left(4\sigma_r \cdot T_m^3\right)^{-1}} \tag{3}$$

As is well known, if the effective Biot number is small ($\overline{Bi} < 0.1$), the conductive resistance is negligible and the heat transfer is primarily dependent on or limited by the external transfer coefficient. For example, this is usually the case with materials of high thermal conductivity subjected to natural convection. To increase the net heat transfer, each of the resistances mentioned in Eq. (1) should be reduced.

Under pure radiative boundary condition, as in space applications, an analogous Conduction-Radiation Number *Nr*, is defined as [7]:

$$Nr = \frac{\text{internal conductive resistance}}{\text{external radiative resistance}} = \frac{4 \cdot \sigma_r \cdot T_m^3 \cdot L_C}{k_{\text{plate}}} \tag{4}$$

In the present work, effort is made to reduce the conductive resistance $R_{th}|_{\text{conduction}}$ of the radiator plate by embedding a PHP in it, as schematically detailed in Fig. 1(b). The pros and cons of such a design are analyzed by experimental and simulation studies. $R_{th}|_{\text{radiation}}$ is generally reduced by increasing the surface emissivity of the radiator by suitable surface coatings. In terrestrial applications, forced convective conditions are suitably used to reduce $R_{th}|_{\text{convection}}$.

2. Experimental details and procedure

The main objectives of the designed experimental setup are as follows:

(i) To generate new information on the applicability of embedded PHP concept in emerging heat transfer applications, especially

focusing on the feasibility of such structures as thermal spreaders/radiators.

(ii) To employ high speed, spatio-temporal infrared thermography to study the thermal performance of embedded PHP radiator plates, under coupled natural convection and radiation heat transfer conditions on the exposed surface.

(iii) To generate data for validation of the 3D computational heat transfer model and to subsequently estimate the effective thermal conductivity of the embedded PHP structure, under different operating conditions.

The experiments were performed on radiator plates made of aluminum and mild steel respectively with dimensions 350 mm × 350 mm × 5 mm, as shown in Fig. 2(a). The respective effective Biot numbers were: aluminum-$\overline{Bi}_z \approx 0.03$; $\overline{Bi}_y \approx 6 \times 10^{-4}$ and mild steel-$\overline{Bi}_z \approx 0.13$; $\overline{Bi}_y \approx 26 \times 10^{-4}$. The effective Biot number $\overline{Bi}_z$ is with reference to the longitudinal length of the embedded portion of the radiator plate (=250 mm), while $\overline{Bi}_y$ is defined with respect to the thickness of the plate (=5 mm). Here, the thermal conductivity values of the respective materials, i.e., MS (=51.4 W/mK) and Al (=235 W/mK), have been used. The average heat transfer coefficient is due to the applicable boundary condition, viz., simultaneous natural convection and radiation on the exposed surface of the radiator plate. The procedure for calculating $\overline{Bi}$ is shown in the Appendix.

Semi-circular grooves were milled on these substrate plates into which a continuous capillary tube made of copper (ID/OD: 2.0/3.0 mm, total length of the tube used = 5570 mm with an internal volume 17.5 cc and an inter tube pitch of 12 mm, having 11 U-turns on each end) was mechanically embedded in the milled groove with the application of a heat sink compound (copper tube was inserted into the milled slot with a mild force by the help of a wooden mallet), as detailed in Fig. 2(a). The exposed top surface of the thermal radiator plate/substrate was coated with a high emissivity $\epsilon \approx 0.96$

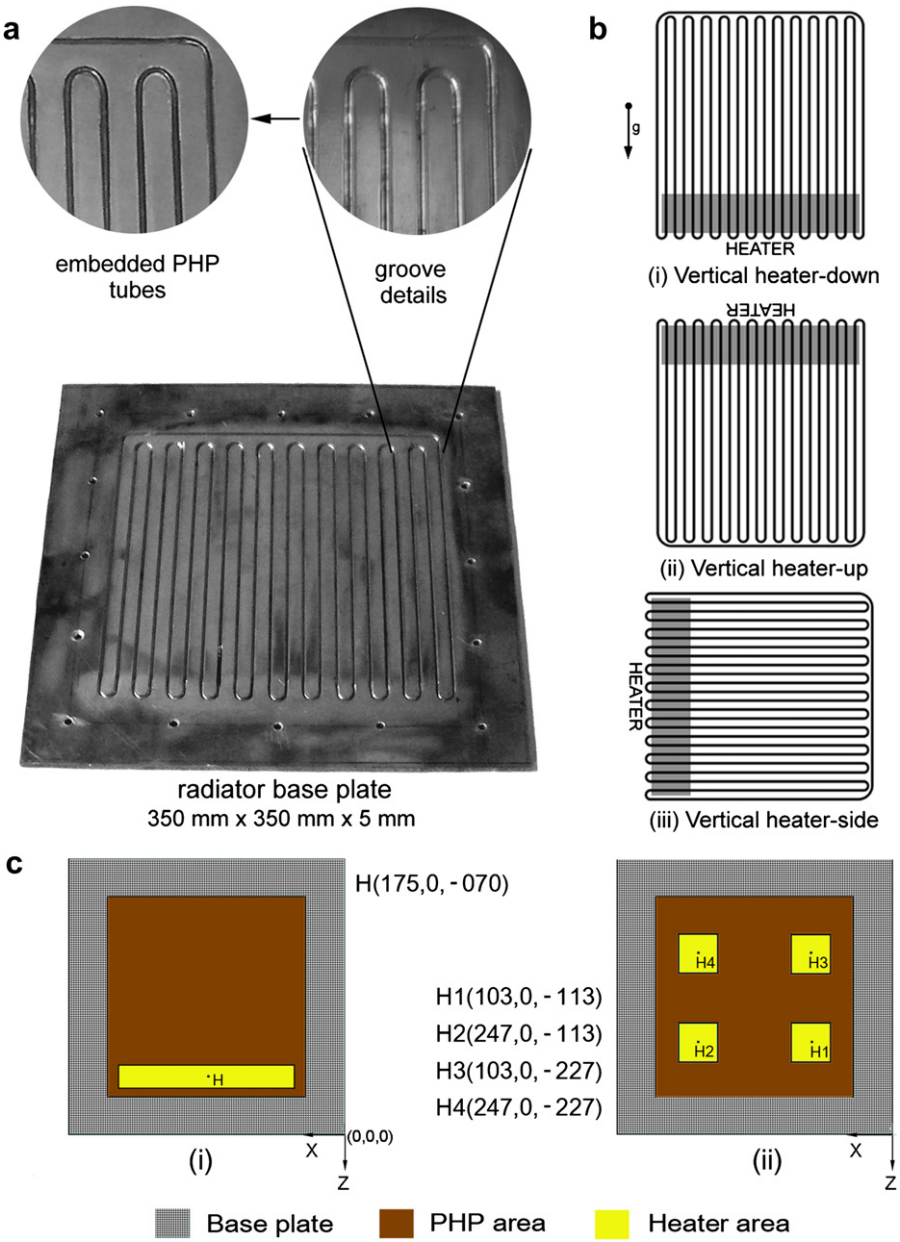

Fig. 2. (a) The exposed surface of the thermal radiator plate with details of the grooves milled on it and the embedded PHP tubes inside the grooves (b) Three different test orientations of the plate, with respect to gravity (c) Physical arrangement and coordinates of the heaters located on the back side of the radiator plate.

Nextel® paint (supplied by M/s Mankiewicz Gebr. and Co.). The setup was erected in a black enclosure to minimize the ambient reflections. The enclosure was open from top and bottom for unhindered natural convective air currents. The PHP embedded radiator plates were mounted on a tilt-able frame to locate in any desired orientation. The thermal performance of the these radiator plates were then tested in the vertical plane, at three different heater orientations with respect to gravity, as depicted in Fig. 2(b).

For single heater experiments, heat supply was provided by a surface mountable flat mica heater (supplied by M/s Minco Inc.) of size 200 mm × 50 mm × 1 mm, centrally mounted on the bottom of the base plate at a distance of 45 mm from the bottom edge. Multiple heater experiments were also performed with surface mountable heaters (50 mm × 50 mm × 1 mm). The geometric details of the heater arrangement are shown in Fig. 2(c). The entire substrate plate was insulated from the back side where the heaters are located (face opposite to the exposed radiating surface). As noted earlier, the boundary condition on the top exposed surface was conjugate, i.e., combined natural convection plus radiation ($\epsilon \approx 0.96$). For DC power input and measurement, a digitally controlled power source coupled with high precision (0.25% FS) digital multimeter, was used. The heat input to the strip heater was varied from 50 W to 150 W (corresponding flux = 5 kW/m^2 to 15 kW/m^2, based on heater size/area).

The evacuation/filling of the PHP was done via a micro-metering valve, which could be fitted to either the vacuum pump (Varian® Turbo-coupled rotary pump; vacuum level typically less than 10^{-4} mbar) or the calibrated working fluid filling pipette. The working fluid was distilled, deionized and degassed water and high purity (99.6%) ethanol, respectively. After proper filling and sealing of the PHP, desired heat input was given to the surface mounted heater(s). All experiments were performed with a volumetric fluid Filling Ratio (*FR*) of 60% (10.5 ml of working fluid was admitted at room temperature). When no PHP action was desired, no working fluid was administered in the tube; the PHP tube was dry and empty, under vacuum.

A high speed, high resolution Forward Looking Infrared Camera (Model: FLIR SC-6000; resolution of 640 × 512 at 120 Hz digital output and sensitivity of 2.5 mK, 3–5 μm) was used to obtain real-time temperature profiles of the exposed surface of the radiator plate. Eight pre-calibrated thermocouples (ungrounded, sheath protected, Type-K, ±0.1 °C after calibration with Pt-100, bead diameter 0.25 mm) were used not only to measure the temperature at important spatial locations on the plate, but also to validate/calibrate the temperature readings obtained by the IR camera. Thermocouple data acquisition was done by a 24-bit PC interface with Labview®. (M/s National instruments, model 'NI-PCI-4351') along with the recording of IR thermography, from commencement of heating till a quasi-steady state was achieved.

3. Results and discussion

The results are based on the 2D spatial variation of temperature of the exposed radiator surface by IR thermography. Before proceeding to discuss the results, it is worthwhile to note that the temperature gradients, in the Y-direction corresponding to the thickness of the substrate (=5.0 mm; for both MS and Al substrates), were negligible, as justified later in Section 3.5. Heat losses from all other sides, except the exposed face, were also minimized to an extent of about 7–10% of the supplied heat. Thus,

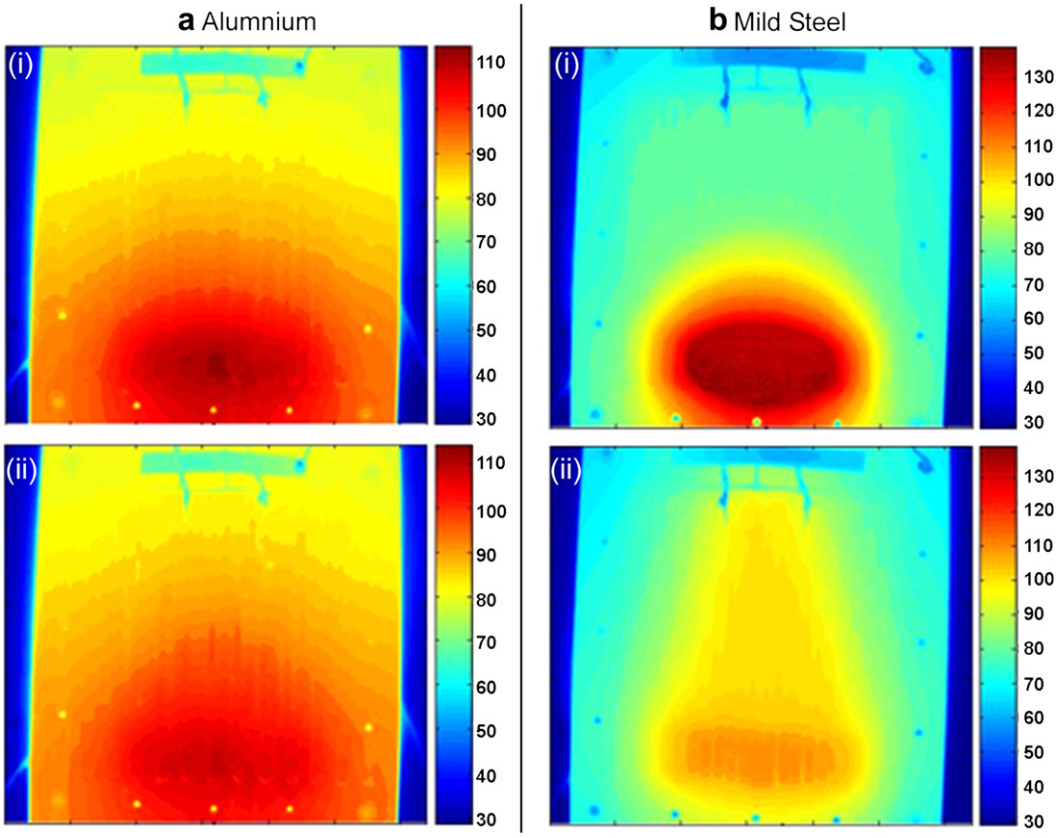

Fig. 3. IR thermographs of the top exposed surface of the radiator plate in vertical heater-down orientation at 120 W heater input power at quasi-steady state operation with ethanol as the working fluid. (a) Aluminum plate (i) without active PHP; dry device, and (ii) with embedded PHP operating, (b) Mild Steel plate (i) without active PHP; dry device, and (ii) with embedded PHP operating.

arguments and conclusions based on the surface temperature of the radiator plate, as measured by the IR camera, are expected to be rational and valid.

3.1. Spatial thermographs

We first discuss the results obtained for the single heater arrangement. Fig. 3(a) shows the temperature profiles of the Al plate at 120 W heat input for vertical heater-down position (Fig. 2(b)(i)), for two cases, (i) dry test (no PHP action) and, (ii) with ethanol as working fluid. Comparing these two cases we note that the degree of isothermalization achieved is rather similar. Similar results were obtained when the working fluid was changed to water. It is evident that the base thermal conductivity of the Al material is so high that further enhancement due to the PHP action is not noticeable. The same conclusion was achieved by the preliminary numerical study of Khandekar and Gupta [2]. The present experiments confirm their finding that the relative contribution of a PHP in enhancing the effective conductivity of the radiator plate in the longitudinal direction is not noticeable/appreciable as the $\overline{Bi}_z$ of the original Al base plate structure is itself rather low.

Arguments based on the theory of enhancement of heat transfer by extended surfaces/fins can also be invoked to understand the behavior of the PHP embedded radiator plate. The theory clearly highlights the asymptotic leveling of fin efficiency with increasing fin thermal conductivity beyond a particular value [8]. Thus, it is clear that, because the heat transfer is governed/limited by the external resistance i.e., convection, radiation or conjugate (Eq. (1) and (2)), the advantage achieved by embedding a PHP in a radiator plate will asymptotically level off for base plate materials with higher thermal conductivity. In other words, we can also state that, it is not advisable to invest in any enhancement technology that increases the thermal conductivity of the base plate beyond a particular techno-economic limit. In this background, PHP structures can prove to be quite advantageous in increasing the effective thermal conductivity of low conductivity materials like mild steel, as we will see next. Although the thermal resistance of PHPs can never be as good as conventional heat pipes, they are much simpler and cheaper to fabricate [5]. Also, PHPs are not affected by conventional heat pipe limitations (e.g., capillary limit).

To further ratify the above arguments, we conducted experiments with radiator plate made of mild steel material. This has a higher effective Biot number, $\overline{Bi}_z \sim 0.13$ because of the low thermal conductivity of MS. The results for the two cases ((i) dry test; no PHP action and, (ii) with ethanol as working fluid), as shown in Fig. 3(b, (i), (ii)), clearly depict the contribution of the embedded PHPs in the isothermalization of the MS radiator plate for a heat input of 120 W (same as that of the Al plate in Fig. 3(a)). It can be seen that, the maximum plate temperature drops by more than 30 °C when the embedded PHP action commences as compared to the dry-device.

A comparison of maximum temperature T_{max} of the two radiator plates, at a given heat input power, also provides a clear indication of the advantage achieved by the PHP action. Fig. 4 shows the maximum temperature of Al and MS plates at different heat inputs. For a given heat input, the values of T_{max} for both the plates are quite comparable, despite the fact that $(\overline{Bi}_z)_{MS} \approx 4(\overline{Bi}_z)_{Al}$. In fact, at high heat loads, when the PHP action is smooth and effective, T_{max} is practically identical for both these plates. This implies that, as regards T_{max}, for a given heat input, the MS plate behaves identically to the Al plate. Therefore, in cases where T_{max} defines the design considerations, a suitable substrate material, which is mechanically superior to aluminum but thermally inferior to it, could very well do the job with embedded PHP tubes for enhanced spatial thermal conductivity. This fact is convincingly proven by these results.

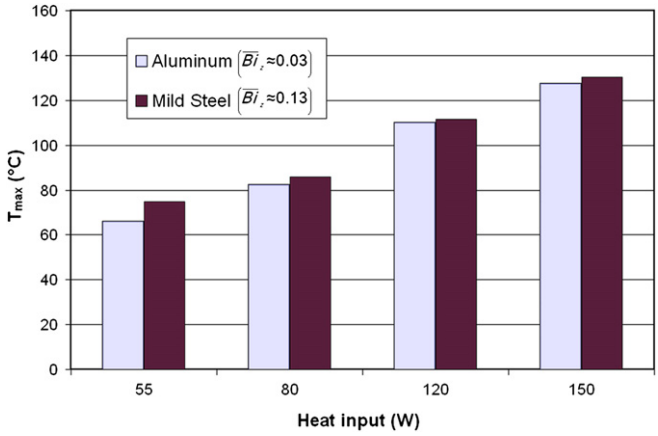

Fig. 4. Comparison of maximum plate temperature, T_{max} for Al and MS plates (vertical, bottom-heating orientation, working fluid: ethanol with $FR = 60\%$).

3.2. Thermal resistance

The thermal resistance of the radiator plate is obtained as:

$$R_{th} = \frac{(T_{max} - T_{min})}{\dot{q}} \tag{5}$$

The thermal resistance of the plate is calculated at different heat inputs, where T_{max} and T_{min} are averaged out for sufficiently long time after quasi-steady state has been achieved. Due to enhanced pulsations of the two-phase working fluid inside the capillary tubes by increasing heat flux [5,9], there is a reduction in the maximum temperature (T_{max}) and increase in the minimum temperature (T_{min}) of the plate, i.e., isothermalization of the spatial gradients takes place. This results in the reduction of the net thermal resistance of the plate.

Fig. 5 shows the variation of the thermal resistance of the embedded radiator plate with increase in heat input for vertical heater-down orientation. The results indicate that R_{th} of such structures decreases with increase in heat flux, which is inline with many earlier observations on PHPs tested under other types of boundary conditions (e.g. [4,10,11]). This is due to the fact that the thermal power input is the driving force for the self-sustained two-phase flow oscillations of the PHP; increasing the heat input power enhances the oscillations leading to enhanced heat transfer.

The decrease in thermal resistance is more significant in the case of MS plate as compared to the Al plate; in the latter only a slight decrease in the resistance is observed, inline with the arguments put forward in Section 3.1. Also, the results are slightly

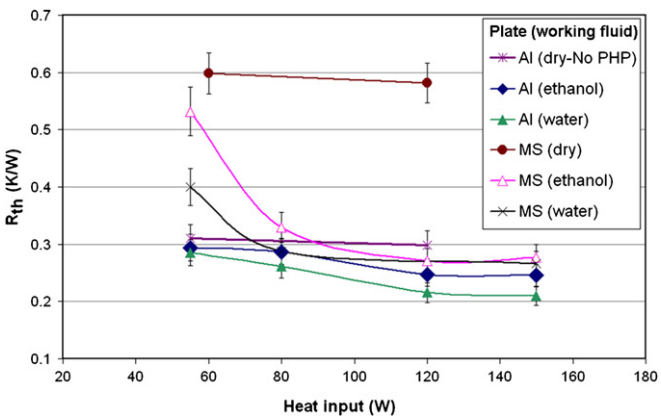

Fig. 5. Variation of overall thermal resistance (R_{th}) of the two thermal radiator plates with heat input power.

better with water as working fluid than ethanol. However, as the heat input increases, the performance of ethanol as the PHP working fluid approaches that of water. Initially, the latent heat of water dominates the heat transfer while at higher heat loads, as the oscillating frequency increases, the convective heat transfer plays the dominant role.

At 55 W input heat power, the pulsations were minimal (as seen by the IR thermographs while performing the experiments) and therefore R_{th} is also higher than at increased heat input. This suppressed pulsating action at low heat loads are also observed and described by Qu and Ma [12]. At higher heat inputs, R_{th} of the MS plate is reduced by almost 50% which reiterates that the PHP is indeed playing a significant role in overall heat transfer share for low thermal conductivity plate materials (high $\overline{Bi}_z$ case).

3.3. Effect of orientation

To study the effect of operating orientation on the thermal performance of the PHP (potential applications may need such composite structures to operate in any orientation; moreover, for space applications, gravity is absent), experiments were also performed for vertical heater-up and vertical side-heating orientations of the plate as detailed earlier in Fig. 2(b).

At lower heat inputs, for vertical heater-up position, gravity adversely affected the performance and only intermittent pulsations (periodic 'start-stop' behavior as described by Yang et al. [6]) were observed. With higher heat inputs, the thermal driving forces could overcome the adverse effect of gravity. The performance improved considerably and pulsations showed up regularly at higher heat inputs, thus reducing R_{th} considerably. Fig. 6(a) shows the snapshots of the MS radiator plate in vertical heater-up position at input heat power of 140 W at two different instants of time. Since the pulsations were intermittent, case (a) (i) and (ii) correspond to the non-pulsating and pulsating mode respectively. It can be seen that T_{max} drops by about 10 °C in the pulsating mode.

The performance of the MS plate in vertical side-heating orientation was also quite satisfactory, with T_{max} comparable to that of vertical bottom-heating orientations (Fig. 3(b) and Fig. 6(b)). The variation of thermal resistance with input heat in this case also followed a similar trend as that of vertical heater-down as can be seen from Fig. 6(c). However, as noted earlier, for vertical heater-up orientation, the pulsating action was not continuous and hence the thermal resistance was comparatively higher. A typical variation of T_{max} at quasi-steady state for different operating orientations with respect to gravity is shown in Fig. 7. The magnitude of T_{max} as well as its amplitude of variation was seen to be high in vertical heater-up orientation as compared to the other two orientations due to the intermittent pulsating operation. In the latter case, the temperature starts rising when the pulsation stops and drops when pulsations re-commence.

3.4. Effective thermal conductivity

3.4.1. Computational modeling approach

As there is no first-principle mathematical model yet available representing the complex PHP thermo-fluidic phenomena [13–15],

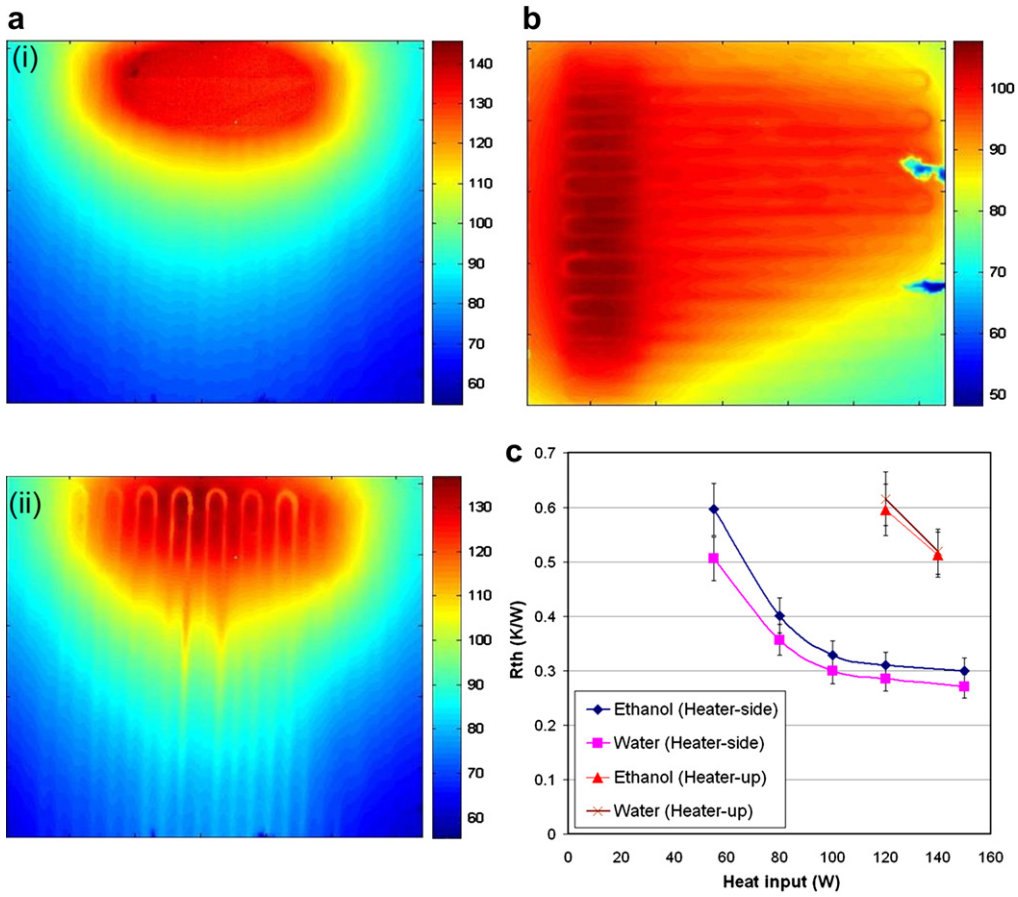

Fig. 6. (a) Instantaneous spatial temperature profiles of the MS plate with intermittent 'start-stop' pulsations mode in vertical heater-up orientation at 140 W with water (i) Non-pulsating 'stop' mode (ii) Pulsating 'start' mode. (for temporal temperature variations for these two states, see Fig. 7) (b) Temperature profile of the MS plate in vertical side-heating orientation at 120 W with ethanol (c) Variation of R_{th} with heat input (vertical heater-up and vertical side-heating orientations).

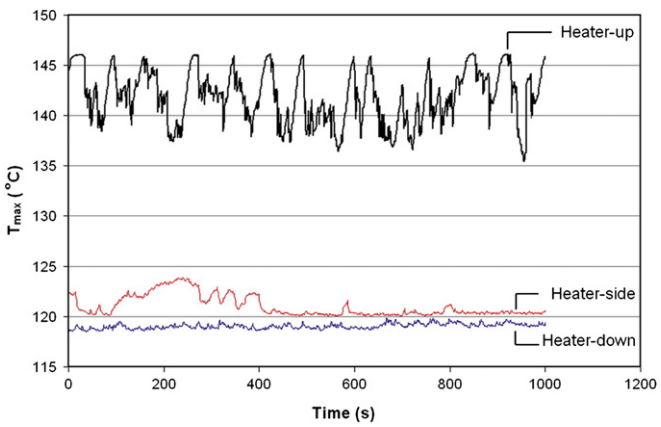

Fig. 7. Variation of T_{max} for the MS plate at quasi-steady state for different orientations of the radiator plate. Heater-down position provide the smoothest operation while in heater-up orientation the PHP runs with intermittent 'start-stop' mode as described by Yang et al. [6].

it is not possible, in a straightforward way, to estimate the enhancement of heat transfer because of such embedded PHP structures in radiator plates. Yet, for furthering engineering applications, an order-of-magnitude estimation of the enhancement is essential and vital for design calculations. In this context, we have attempted to get a working range of the effective thermal conductivity of the embedded PHP structure. It is emphasized that such an approach only provides working estimates and can, in no way, substitute for a detailed first-principle model, which remains an active field of research [15,16]. The methodology adopted herein, for the estimation of effective thermal conductivity rendered by the embedded PHP tubes, is described below:

(i) For a given global orientation of the radiator plate and heat power input to the heater, the quasi-steady state spatial distribution of temperature were recorded by the IR camera. This exercise was done under two conditions (a) Dry test, when the PHP tubes were completely evacuated and no working fluid is present i.e. no enhancement of the thermal conductivity of the radiator plate and, (b) when the PHP tubes were filled with 60% by volume of the working fluid so that the PHP is operational, rendering enhanced effective thermal conductivity to the radiator plate, as has been described earlier.

(ii) Once the experimental database, as described in (i) above, was generated, 3D numerical heat transfer simulations were performed on a computation domain representing the physical experimental setup, with the relevant boundary conditions. Simulations were performed on two different 3D models which differed only in the degree of details of the physical experimental domain. The first was a simplistic 'unit-cell' model representing a single pitch length of the embedded PHP tube, as detailed in Fig. 8. The second model was a detailed approach representing the full experimental domain of the radiator plate, as shown in Fig. 9. The computational domain of both these models consisted of three-dimensional tetrahedron grids (1.15 and 3.77 million cells on the computational domain, respectively, equivalent to node spacing of 1.0 mm on the physical domain) and we solved the energy equation on a commercial platform (Fluent® Version 6.3.26). The absolute convergence criterion set for energy equation was 10^{-8}. Distinction was made between the grid volume corresponding to the radiator base plate material and the grid volume corresponding to the embedded tubes of PHP. The applied boundary conditions are also shown in Figs. 8 and 9, which are inline with the actual experimental conditions. All simulations have been conducted with a mild steel base plate. Following additional assumptions are also made:

- The material of each region is isotropic, homogenous and with constant thermal properties.
- Perfect contact is maintained at the interface of two dissimilar materials.
- All the edge planes of the control volume are insulated (for the unit-cell model (Fig. 8), both the planes in the longitudinal direction have symmetric boundary conditions).
- At the upper surface, combined heat transfer boundary condition i.e. natural convection (with $h = 5.5$ W/m^{2}K at 55 W to 8 W/m^{2}K at 150 W), following well known Nusselt

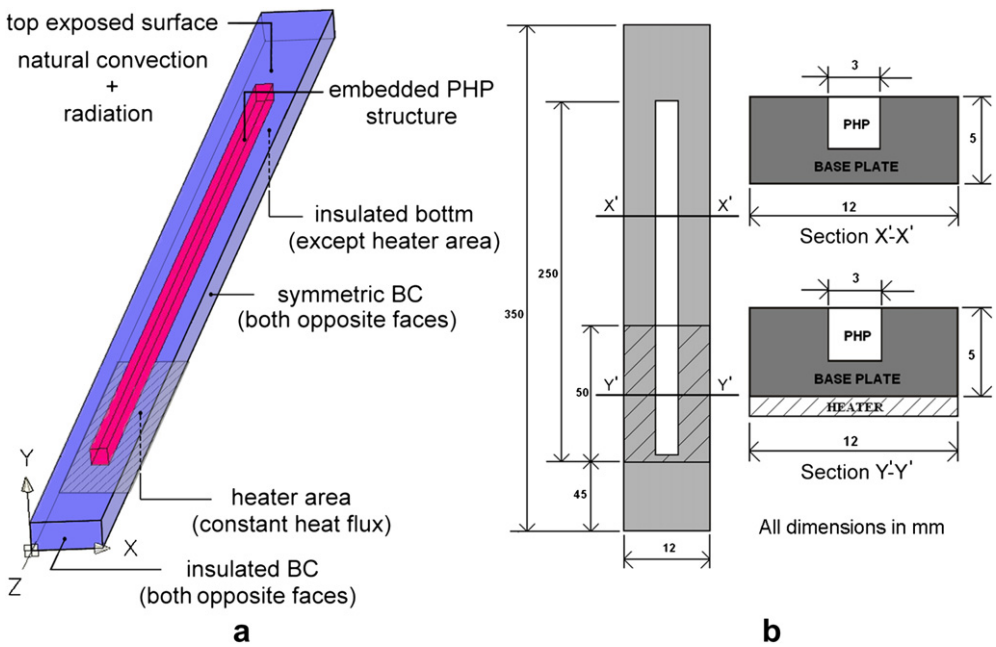

Fig. 8. (a) 3D geometry of the simple unit-cell model along with the applied boundary conditions, (b) Dimensional details of the model.

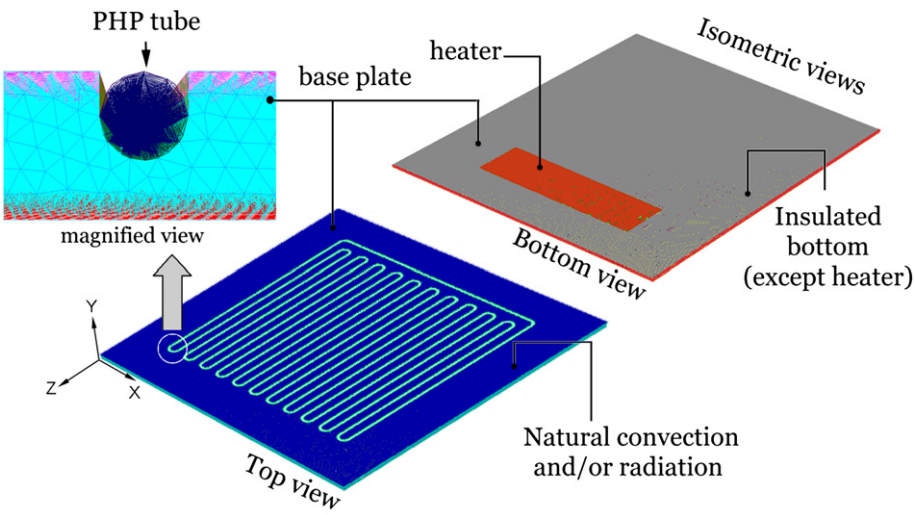

Fig. 9. 3D geometry of the full-domain model along with the applied boundary conditions.

number estimates for vertical plates [17] with radiation ($\epsilon = 0.96$) boundary condition is applied. The lower surface is insulated except at heater locations, where a constant heat flux boundary condition is specified.

To commence the computations, the grid volume corresponding to the PHP tubes was initially assigned an arbitrarily higher thermal conductivity than the MS base plate. For a specified thermal conductivity of these PHP tubes, the temperature profiles obtained

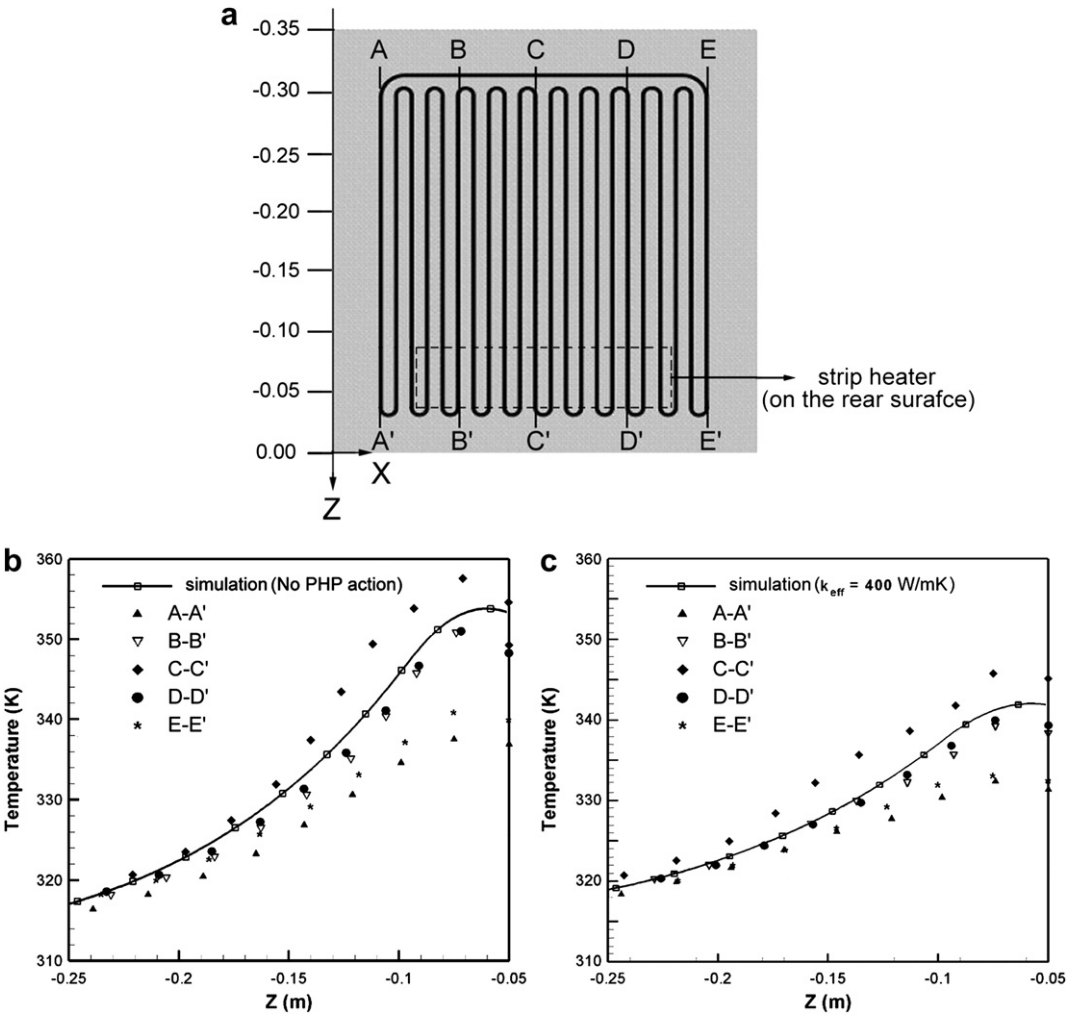

Fig. 10. (a) Experimental surface temperature profiles at five locations on the X axis (along the negative Z axis) are compared with the unit-cell simulation model (b) comparison when no PHP action occurs (no working fluid inside the system) (c) comparison when the PHP is operating. In both cases the heater input power is 55 W.

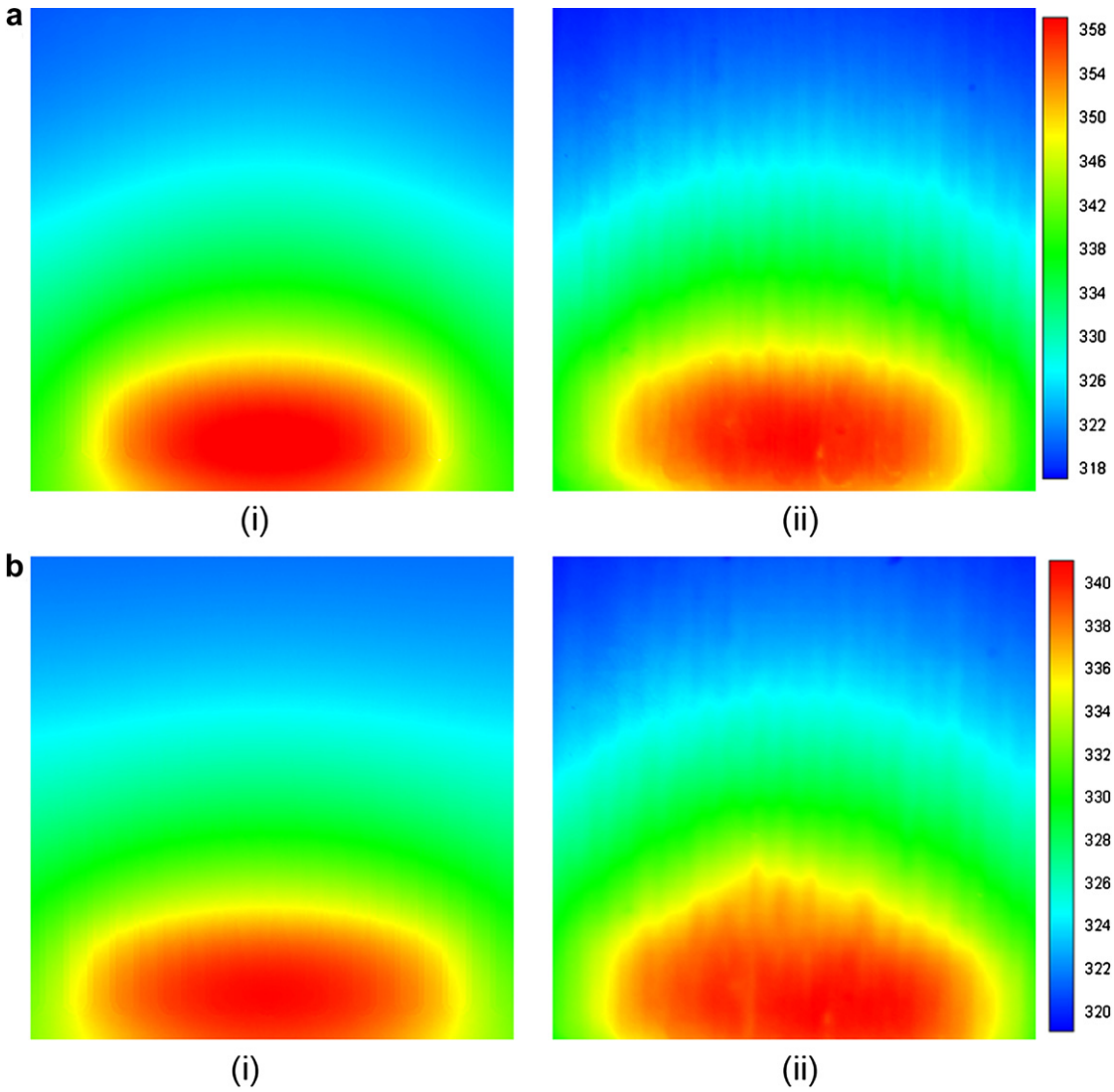

Fig. 11. Comparison of experimental and simulated thermal profiles at 55 W input heat power (a) Dry test (No PHP action) (i) simulated profile (ii) corresponding experimental profile; (b) With PHP action (i) simulated profile with $k_{eff} = 600$ W/mK (ii) corresponding experimental profile.

by simulation on the top surface of the computational domain were then compared with the experimental temperature profiles of different tubes across the plate. For doing this comparison of longitudinal temperature profiles obtained from experiments and simulations, five line traces on the exposed surface of the radiator plate were chosen, as depicted in Fig. 10(a). It will be appreciated that while corner effects are inherent in the experimental system, the simplistic unit-cell symmetric representation of the experimental system in the computational domain (as depicted in Fig. 8) will not be able to capture these corner effects. Therefore, we have used line-traces, B–B′ and D–D′, for comparison and subsequent estimation of effective thermal conductivity of the radiator plate for the simplistic unit-cell model. Hence, there will be some deviation between the simulated line temperature profile and the experimental profiles at A–A′, C–C′ and E–E′. To capture the corner effects and obtain a better estimation of the effective thermal conductivity, a full domain simulation study was undertaken, as described earlier in Fig. 9. The only control variable was the thermal conductivity of the embedded PHP tubes, which was iteratively changed in the simulations until the simulated results provided a reasonable fit to the trend obtained across the radiator plate. Thus, an engineering estimate of the effective thermal conductivity of the embedded PHP tubes could be ascertained.

3.4.2. Model validation experiments

Before applying the effective thermal conductivity modeling approach, as described above, simple validation experiments were performed on dry radiator plates (no PHP action). In such a system, heat transfer takes place in pure diffusional mode through the composite radiator plate, before getting lost to the environment by the combined action of natural convection and radiation from its exposed top surface. Once the validity of the model was benchmarked by the dry tests, the simulations were then compared with the working PHP to determine the effective thermal conductivity of the composite system, as has been explained in Section 3.4.1.

For the unit-cell model, under no PHP action, Fig. 10(b) shows the comparison of experimental and simulated temperature profiles at various locations for a heat input of 55 W. It can be seen that there is satisfactory correlation between the predicted temperature profiles along traces B–B′ and D–D′, to the corresponding experimental data. As expected, the experimental temperature profile along C–C′ is marginally higher (~1.5%) and

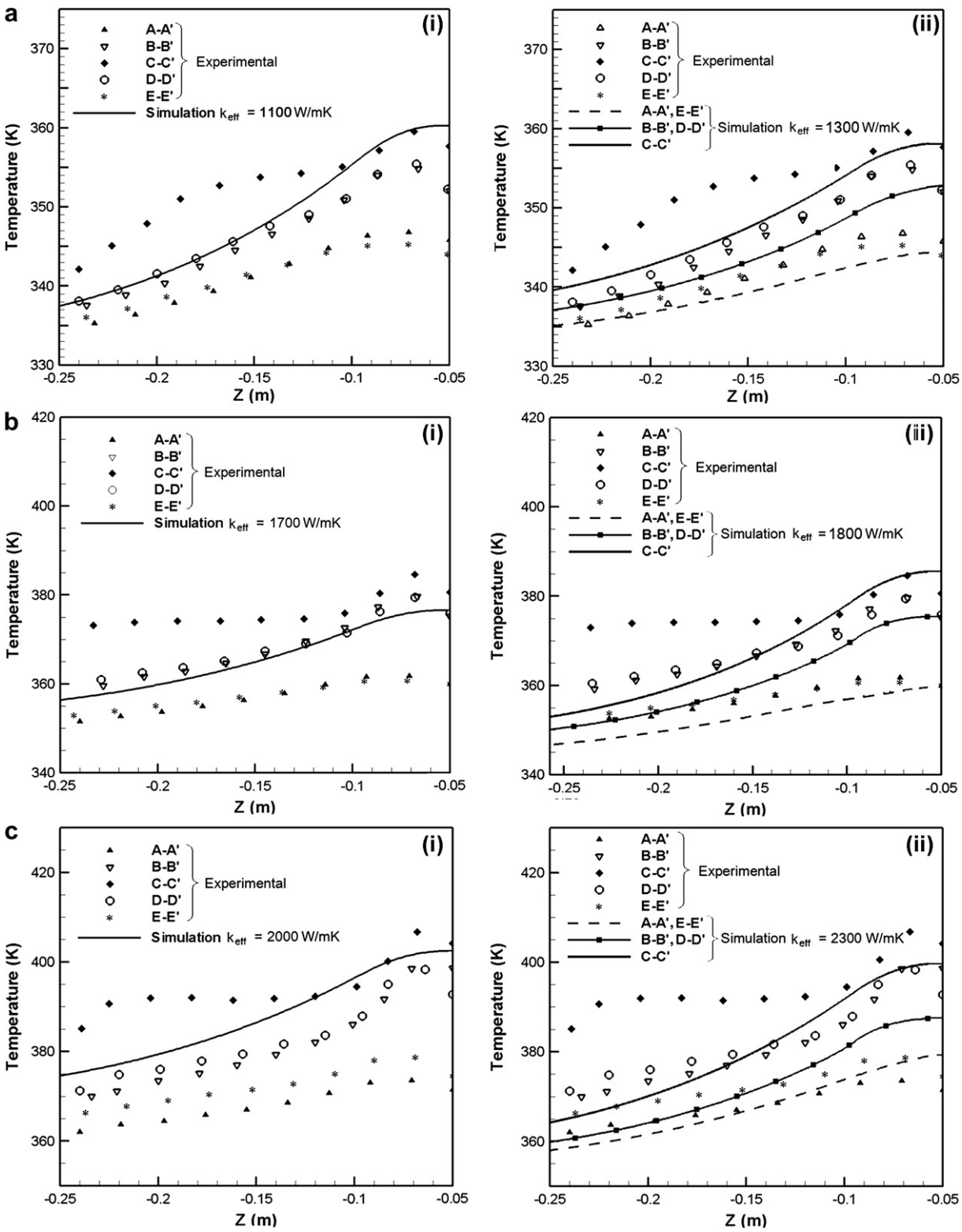

Fig. 12. Estimation of effective thermal conductivity of the plate at heat inputs (a) 80 W (b) 120 W (c) 150 W with ethanol as working fluid, for (i) unit-cell simulation; (ii) corresponding full-domain simulation.

that along A–A′ and E–E′ is somewhat lower (~5.0%) than the simulated profile. Three validation tests were conducted at 55 W, 80 W and 120 W with no PHP action; in all the three cases, the model satisfactorily predicted the temperature profile along B–B′ and D–D′, while the discrepancies at other locations never exceeded 7%. Similar validation exercise for the dry radiator plate was also done for the full domain model for various heat inputs; sample results of this validation exercise at 55 W input power, showing the comparison of experimental and simulated surface temperature profiles, are shown in Fig. 11(a).

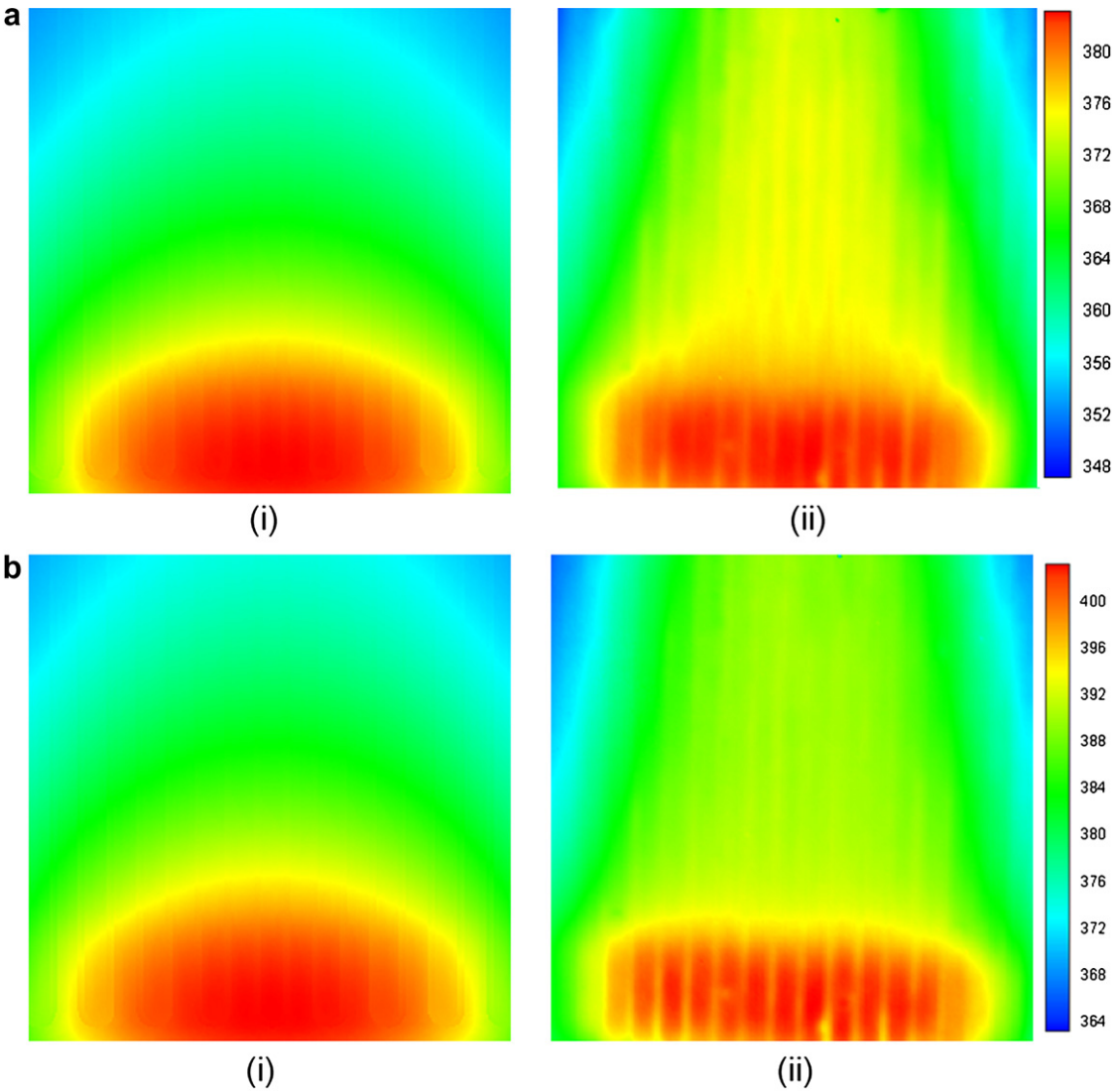

Fig. 13. Comparison of experimental and simulated thermal profiles with working embedded PHP at different heat inputs (a) at 120 W input power (i) simulated with $k_{eff} = 1800$ W/mK (ii) corresponding experimental profile (b) at 150 W input power (i) simulated with $k_{eff} = 2300$ W/mK (ii) corresponding experimental profile.

3.4.3. Estimation of effective thermal conductivity

Post validation, the thermal conductivity of the volume represented by the embedded PHP was increased in the simulations till the temperature profiles matched with the experimental data, under identical boundary conditions. The results for 55 W heat input, for unit-cell and full domain simulations, are shown in Figs. 10(c) and 11(b) respectively (for direct comparison with corresponding dry test validation results, as described in the previous section). As can be seen from the data, the PHP action immediately brings the maximum plate temperature down while the minimum temperature is somewhat increased.

Fig. 12a(i), b(i) and c(i) show the comparisons of experimental and simulated temperature profiles for a working PHP for the unit-cell model at different heat inputs, while Fig. 12a(ii), b(ii) and c(ii) show the comparisons for the corresponding results of the full domain model. For lower heat inputs, the profiles show a similar trend across the plate with nearly the same values of T_{max} and T_{min}. In the unit-cell model, for higher heat inputs, the discrepancies in the experimental and simulated line profiles were higher. These discrepancies were minimized in the full domain simulation. For the experimental temperature profiles, the isotherms in the central portion of the plate 'peak' up. This pronounced isothermalization of the central portion of the plate under experimental conditions cannot be captured by a simplistic effective thermal conductivity approach. It should be kept in mind that the internal two-phase phenomena of a PHP are highly complex and there is considerable temporal variation of the 'effective thermal conductivity' rendered by each tube section [4]. Fig. 13, which shows the comparison of experimental and simulated spatial temperature profiles of the full domain model, also pictorially highlights this discrepancy which results in the peaking up of line trace C–C′. While the approach followed in the present simulation work only provides an average effective thermal conductivity value that such systems may possess under the applied boundary conditions, nevertheless it is an important quantity for the designers to know, so as to ascertain the expected thermal performance from such embedded PHP systems.

With higher heater powers, the thermal performance of PHP improves considerably and effective thermal conductivity of the order of 2300 W/mK is achieved (as can be seen in Fig. 12). In the earlier preliminary simulation study of Khandekar et al. [2] too, which was done for multi-heater arrangement, effective thermal conductivity of the order of 2000 W/mK was reported. The present estimates are compared with the earlier results of [2] in Fig. 14, which match quite well, especially at higher flux levels.

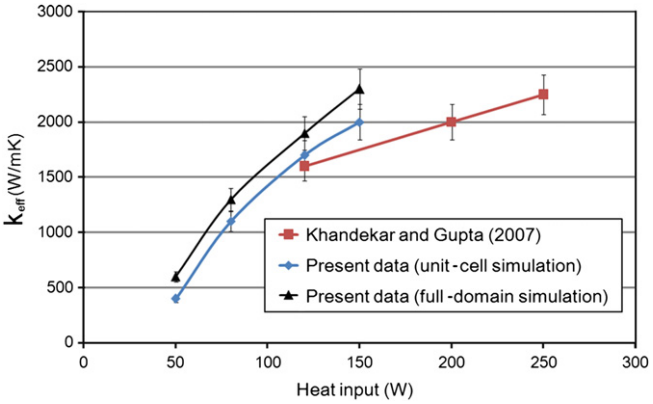

Fig. 14. Variation of effective thermal conductivity (k_{eff}) of the embedded PHP with heat input for the present range of experiments in vertical heater down position and its comparison with preliminary simulations done by Khandekar and Gupta [2] for vertical orientation.

3.5. Transverse temperature profiles (along Y direction)

The entire analysis presented above was carried out based on the surface temperature measurements of the radiator plate base plate (i.e. on X-Z plane, Y = 5). The justification of this approach is only valid provided the temperature gradients in the thickness of the plate are not appreciable (in the Y direction, as per Fig. 1(b)). Fig. 15 shows the temperature profiles across the thickness of the MS plate (on X–Y plane midway through the strip heater) for increasing values of effective thermal conductivity of the PHP structure at a heat input of 150 W (maximum heat input, worst case scenario). The maximum temperature drop observed was negligible with a value of $T \sim 0.8\,^{\circ}$C. This was also independently ratified by the thermocouple readings wherein the maximum gradient in the plate thickness never exceeded 1 °C (for mild steel plates, 150 W heater power). For aluminum radiator, the gradients were considerably smaller. Thus, it can be safely concluded that the use of surface temperature profiles by infrared camera to support the arguments put herein, are justified as the effective Biot number in the Y direction is low enough ($\overline{Bi}_y \approx 26 \times 10^{-4}$) for doing a lumped behavior of temperature in this direction.

3.6. Effect of multiple heaters

Experiments with multiple heaters were carried out to make a qualitative assessment of the thermal performance of the system for asymmetric heating conditions. A total of four heaters were used, in different combinations and IR images of the MS plate were obtained at quasi-steady state. The PHP filling ratio was maintained at 60%. Power given to each heater was 40 W (corresponding flux 16 kW/m^2, based on heater area). Four experiments were carried out, in both gravity and anti-gravity orientations, with power input given to one, two, three and four heaters, respectively. Dry tests

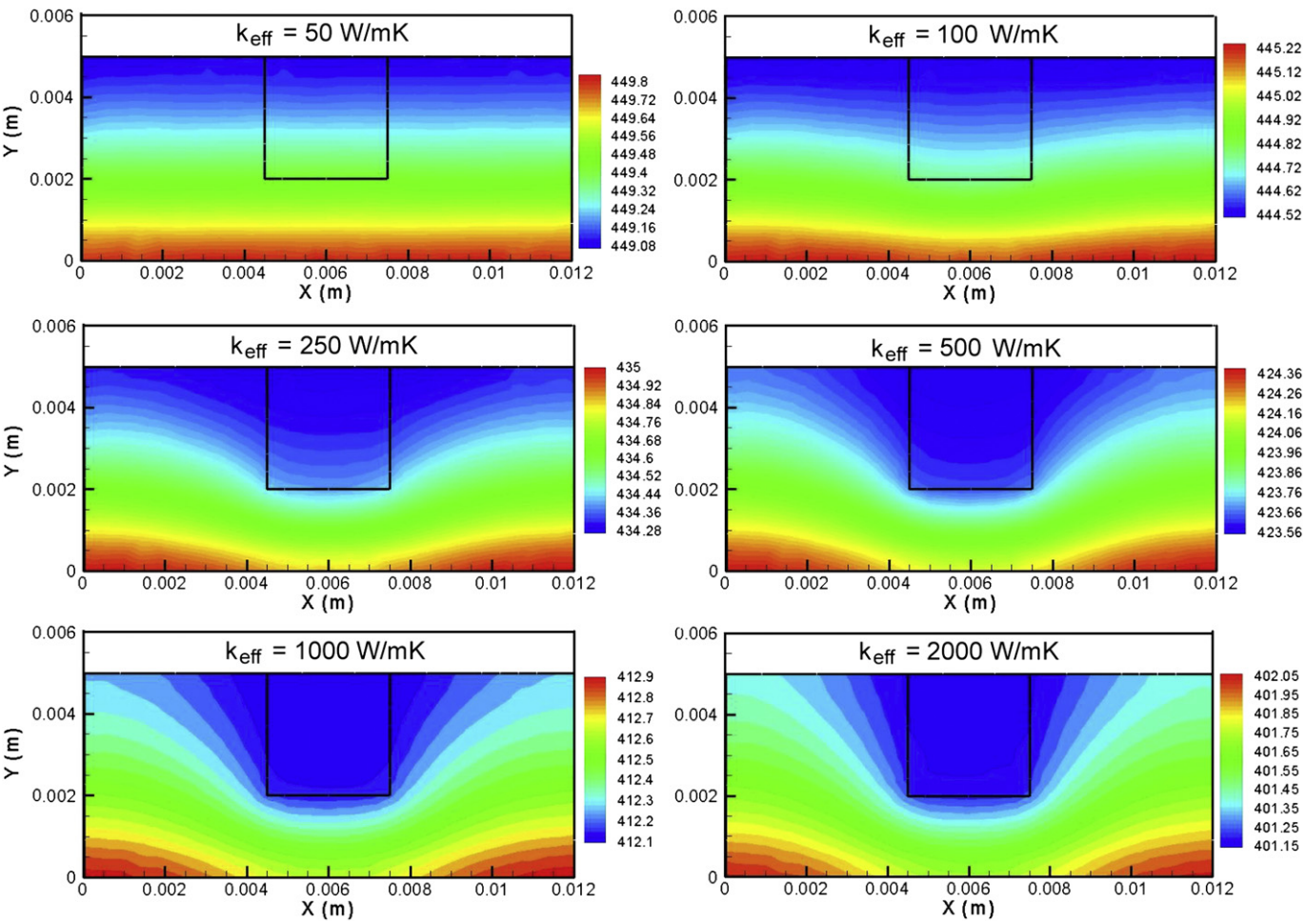

Fig. 15. Temperature (K) profiles along the thickness of the plate (X–Y plane midway through the heater) for increasing value of effective thermal conductivity k_{eff} from 50 to 2000 W/mK. The maximum temperature difference between the surface and the base is of the order of ~0.7 °C (corresponding to k_{eff} = 50 W/mK) or lower.

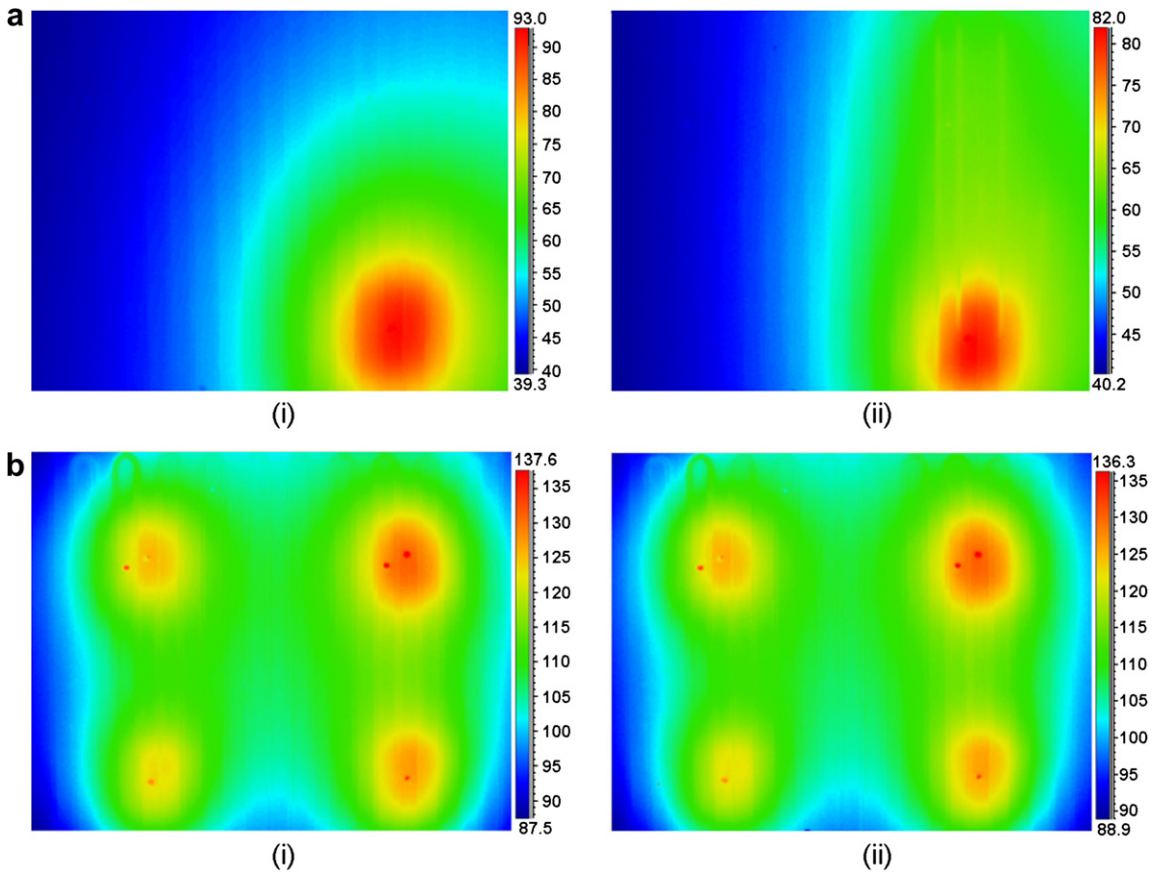

Fig. 16. Comparison of experimental thermal profiles with multiple heaters at 40 W heat input to each heater; vertical orientation. (a) single heater, and (b) with four heaters for (i) dry test (no PHP action) (ii) with PHP action.

were also performed with evacuated tubes and no PHP action. Fig. 16 shows the temperature profiles for dry test and PHP action for 2 heaters and 4 heaters respectively. Fig. 17 compares T_{max} obtained in each case. The difference in T_{max} in dry test and with working PHP is higher in case of single heater and gradually decreases as number of heaters is increased. This is because, as the number of heaters is increased, the distribution of heat flux is inherently more uniform over the entire plate, and thus the specific contribution of the embedded PHP in enhancing the heat transfer in not observable.

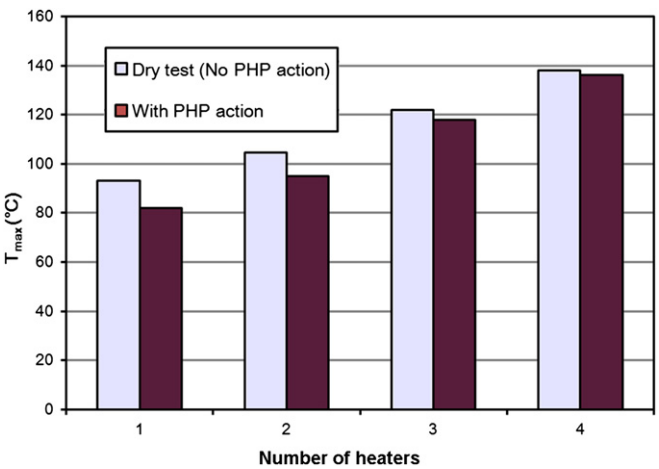

Fig. 17. Comparison of T_{max} for MS plate, dry tests and working PHP with multiple heaters (vertical, working fluid: ethanol with $FR = 60\%$).

4. Summary and conclusions

High heat flux density in modern electronic equipment, including space and terrestrial sectors, demands an effective thermal management system. Pulsating heat pipes have emerged as promising candidate which can cater to both these sectors. With this background, a PHP structure, embedded in a radiator substrate plate, has been experimentally and numerically studied under conjugate boundary conditions. Infrared thermography was employed to study the spatio-temporal performance of the radiator plates.

The following are the major conclusions of the study:

- In those situations where external heat transfer coefficient limits the net heat throughput (i.e. cases like natural convection, where external 'h' is low or pure radiation BC), the thermal conductivity of the base plate on which a heat pipe (conventional or PHP) is embedded does not play a major role in improving the overall heat transfer scenario, after a particular minimum value of its effective thermal conductivity is attained. In the present case, the aluminum radiator plate itself was doing a good enough job. If the base plate thermal conductivity is low, the relative advantage achieved by embedded PHP systems is appreciably higher, as was seen with the high $\overline{Bi}_z$ case, i.e., in case of the mild steel base plate, where the act of embedding a PHP resulted in considerable decrease in its

overall thermal resistance. Such a situation may arise if composite materials, which are mechanically superior to aluminum but thermally inferior, are being proposed as construction elements, especially for the space sector. In addition, for terrestrial applications too, embedded PHPs structures will be attractive in conjunction with low thermal-conductivity base plate materials.

- As the thermal conductivity of the base plate increases ($\overline{Bi}_z$ decreases) and the heat transfer is mainly governed by the external heat transfer coefficient (e.g. in the case of aluminum base plate), the base plate/substrate itself does a god job and further addition of PHP only marginally increases the heat transfer efficiency.
- The T_{max}, in the case of aluminum and mild steel plates, were comparable at higher heat fluxes. Therefore, if T_{max} governs the design considerations, the behavior of both the plates was seen to be comparable. Again, in such cases, a composite material having a weight/strength advantage over aluminum but thermally inferior could be considered as an option. The span-wise thermal conductivity of such a composite may be tailored by suitably embedding a PHP structure.
- The effect of orientation of the plate on its thermal performance was also studied. The operating inclination angle of the PHP tubes affects overall heat transfer characteristics. These changes can be attributed to the change in the internal flow patterns and pulsating action [9]. Increasing heat flux makes these performances comparable.
- Simulations also indicate that relative advantage of any enhanced thermal conductivity device embedded in a radiator plate (such as heat pipes, PHPs etc.) will decrease, as the absolute value of thermal conductivity of the enhancement device/structure increases beyond a particular value. This is inline with the extended surface heat transfer analogy.
- The order-of-magnitude of effective thermal conductivity achievable by PHP ranges from 400 W/mK–2300 W/mK, depending on the heat flux applied; increasing with increasing the applied heat flux. These values are sufficiently attractive for its use as embedded structures in thermal radiator systems.

Acknowledgements

The research is partially funded by Indian Space Research Organization, Space Technology Cell IIT Kanpur (No: #ISRO/ME/20050083) and Board of Research for Nuclear Sciences, Department of Atomic Energy, Government of India (N: #IITK/ME/20050292). Thanks are also due to Mr. D. R. Bhandari and Mr. P. P. Gupta from ISRO Satellite Center, Bangalore and Mr. Pavan Sharma from Reactor Safety Division, Bhabha Atomic Research Center, for their constructive suggestions. The IR camera was procured by funds granted by the Department of Science and Technology, Government of India (FIST Scheme). Additional experiments conducted by Anjani Kumar Varshney, under the IITK-SURGE-2010 fellowship are also acknowledged.

Nomenclature

$\overline{Bi}$	effective Biot number
D	diameter (m)
FR	volumetric filling ratio (V_{liq}/V_{total})
g	acceleration due to gravity (m/s^2)
h	heat transfer coefficient (W/m^{2}k)
k	thermal conductivity (W/mk)
L	length (m)
$\dot{q}''$	heat flux (W/m^2)
$\dot{q}$	heat input (W)
R_{th}	thermal resistance per unit area (Km^2/W)
T	temperature (°C or K)

Greek symbols

ε	surface emissivity
ρ	density (kg/m^3)
σ_r	Stefan-Boltzman Constant = 5.67e-8 (W/m^{2}K^4)

Subscripts

∞	ambient
c	characteristic
liq	liquid
max	maximum
min	minimum
s	solid

Appendix

The effective Biot number ($\overline{Bi}$) was calculated for the PHP system under, (i) dry configuration (no working fluid in the PHP tubes) and, (ii) with normally working PHP. This was done by calculating the effective heat transfer coefficient as follows:

$$h_{eff} = q''/(T_{avg} - T_\infty) \tag{A1}$$

The $\overline{Bi}$ was then calculated as:

$$\overline{Bi} = h_{eff}L/k \tag{A2}$$

To calculate the reduction in $\overline{Bi}$ due to the PHP action, the k in the above equation was replaced by the k_{eff} values obtained by numerical simulations, validated against 2D spatial distribution of temperature on the radiator plate.

For Al base plate; for a heat input of 150 W.

$$h_{eff} = \frac{150}{0.25 \times 0.255 \cdot (107 - 22)} = 27.68\ W/m^2K \tag{A3}$$

$$\overline{Bi}_z = \frac{27.68 \times 0.25}{235} = 0.03 \tag{A4}$$

$$\overline{Bi}_y = \frac{28.23 \times 0.005}{235} = 6 \times 10^{-4} \tag{A5}$$

For MS base plate; for a heat input of 150 W.

$$h_{eff} = \frac{150}{0.25 \times 0.255 \cdot (110 - 20)} = 26.14\ W/m^2K \tag{A6}$$

$$\overline{Bi}_z = \frac{26.14 \times 0.25}{51.4} = 0.13 \tag{A7}$$

$$\overline{Bi}_y = \frac{26.66 \times 0.005}{51.4} = 25 \times 10^{-4} \tag{A8}$$

References

[1] D.G. Gilmore, Spacecraft Control Handbook, In: Fundamental Technologies, second ed., vol. 1, The Aerospace Corporation (AIAA Publication), 2002.
[2] S. Khandekar, and A. Gupta, Embedded pulsating heat pipe radiators, 14th International Heat pipe Conference (14th IHPC), Florianopolis, Brazil, 2007.
[3] H. Akachi, F. Polášek and P. Štulc, Pulsating heat pipes, Proc. 5th International Heat Pipe Symposium, Melbourne, Australia, 1996, pp. 208–217.
[4] S. Khandekar, N. Dollinger, M. Groll, Understanding operational regimes of pulsating heat pipes: an experimental study, Appl. Therm. Eng. 23 (6) (2003) 707–719.
[5] S. Khandekar, Thermo-hydrodynamics of Closed loop pulsating heat pipes, Ph.D. dissertation, Universitaet Stuttgart, Germany, 2004.

[6] H. Yang, S. Khandekar, M. Groll, Performance characteristics of pulsating heat pipes as integral thermal spreaders, Int. J. Therm. Sci. 48 (4) (2009) 815–824.
[7] M. Kaviany, Principles of Heat Transfer. Wiley- Interscience, 2001.
[8] F.P. Incropera, D.P. DeWitt, Fundamentals of Heat and Mass Transfer, fourth ed. John Wiley and Sons (SEA) Pte Ltd, 1998.
[9] J.L. Xu, Y.X. Li, T.N. Wong, High speed flow visualization of a closed loop pulsating heat pipe, Int. J. Heat Mass Transfer 48 (2005) 3338–3351.
[10] M. Hosoda, S. Nishio, R. Shirakashi, Study of meandering closed-loop heat transport device, JSME Int. J. Ser. B. 42 (4) (1999) 737–743.
[11] B. Tong, T. Wong, K. Ooi, Closed loop pulsating heat pipe, Appl. Therm. Eng. 21 (18) (2001) 1845–1862.
[12] W. Qu, H.B. Ma, Theoretical analysis of startup of a pulsating heat pipe, Int. J. Heat Mass Transfer 50 (2007) 2309–2316.
[13] L. Vasiliev, Heat pipes in modern heat exchangers, Appl. Therm. Eng. 25 (2005) 1–19.
[14] S. Khandekar, and M. Groll, Insights into the performance modes of closed loop pulsating heat pipes and some design hints, Proc. 18th Natl. & 7th ISHMT-ASME Heat and Mass Transfer Conf., Guwahati, India, January 4–6, 2006.
[15] Y. Zhang, A. Faghri, Advances and unsolved issues in pulsating heat pipes, Heat Transfer Eng. 29 (2008) 20–44.
[16] S. Khandekar, P.K. Panigrahi, F. Lefèvre, J. Bonjour, Local hydrodynamics of flow in a pulsating heat pipe: a review, Frontiers in Heat Pipes 1 (2010) 023003 (1–20).
[17] S.W. Churchill, H.H.S. Chu, Correlating equations for laminar and turbulent free convection from a vertical plate, Int. J. Heat Mass Transfer 18 (11) (1975) 1323–1329.